27. Scott NA, Cipolla GD, Ross CE *et al*. Identification of a potential role for the adventitia in vascular lesion formation after balloon overstretch injury of porcine coronary arteries. *Circulation* 1996; 93: 2178–2187.
28. Shi Y, O'Brien JE, Fard A *et al*. Adventitial myofibroblasts contribute to neointimal formation in injured porcine coronary arteries. *Circulation* 1996; 94: 1655–1664.
29. Kramann R, Couson S, Neuss S *et al*. Exposure to uremic serum induces a pro-calcific phenotype in human mesenchymal stem cells. *Arterioscler Thromb Vasc Biol* 2011; 31: e45–e54.
30. Powell DW. Myofibroblasts: paracrine cells important in health and disease. *Trans Am Clin Climatol Assoc* 2000; 111: 271–292. discussion 292–293
31. Gross ML, Meyer HP, Ziebart H *et al*. Calcification of coronary intima and media: immunohistochemistry, backscatter imaging, and x-ray analysis in renal and nonrenal patients. *Clin J Am Soc Nephrol* 2007; 2: 121–134.
32. Hamill KJ, Kligys K, Hopkinson SB *et al*. Laminin deposition in the extracellular matrix: a complex picture emerges. *J Cell Sci* 2009; 122: 4409–4417. (Pt 24)
33. Feaver RE, Gelfand BD, Wang C *et al*. Atheroprone hemodynamics regulate fibronectin deposition to create positive feedback that sustains endothelial inflammation. *Circ Res* 2010; 106: 1703–1711.

Received for publication: 8.8.2011; Accepted in revised form: 11.10.2011

Nephrol Dial Transplant (2012) 27: 2702–2711
doi: 10.1093/ndt/gfr670
Advance Access publication 13 December 2011

Periostin: novel tissue and urinary biomarker of progressive renal injury induces a coordinated mesenchymal phenotype in tubular cells

Bancha Satirapoj[1,2], Ying Wang[1], Mina P. Chamberlin[1], Tiane Dai[1], Janine LaPage[1], Lynetta Phillips[1], Cynthia C. Nast[1,3] and Sharon G. Adler[1]

[1]Los Angeles Biomedical Research Institute, Harbor-UCLA, Torrance, CA, USA, [2]Division of Nephrology, Phramongkutklao Hospital and College of Medicine, Bangkok, Thailand and [3]Cedars-Sinai Medical Center, Los Angeles, CA, USA

Correspondence and offprint requests to: Sharon G. Adler; E-mail: sadler@labiomed.org

Abstract

Background. Periostin acts as an adhesion molecule during bone formation. Knowledge of its expression in kidney injury is scant.

Methods. We investigated periostin function and expression *in vivo* in Sprague–Dawley rats after 5/6 nephrectomy (Nx), in DBA2J mice with streptozotocin-induced diabetic nephropathy (SZ-DN) and unilateral ureteral obstruction (UUO) and *in vitro* in mouse distal collecting tubular cells (MDCT) and in tissue and urine from chronic kidney disease (CKD) patients.

Results. Periostin messenger RNA was increased after 5/6Nx and SZ-DN demonstrating generalizability of the increment in renal injury. Periostin was expressed predominantly in distal tubule (DT) epithelial cell cytoplasm *in situ*, in cells shed into the lumen, and, in lesser abundance, in glomeruli undergoing obsolescence, arterioles and in the tubulointerstitium in extracellular and intracellular locations. In affected DT after 5/6Nx, periostin expression appeared *de novo*, E-cadherin became undetectable and tubule cells displayed the mesenchymal marker proteins fibroblast-specific protein-1 (FSP1) and matrix metalloproteinase-9 (MMP9). Periostin overexpression in cultured MDCT cells dramatically induced MMP9 and FSP1 protein and suppressed E-cadherin. Periostin short interfering RNA blocked these changes. Urine periostin excretion increased over time after 5/6Nx, and it was also excreted in the urine of CKD patients. Urine periostin enzyme-linked immunosorbent assay at a cutoff of 32.66 pg/mg creatinine demonstrated sensitivity and specificity for distinguishing patients with CKD from healthy people (92.3 and 95.0%, respectively) comparing favorably with urine neutrophil gelatinase-associated lipocalin.

Conclusion. These data demonstrate that periostin is a mediator and marker of tubular dedifferentiation and a promising tissue and urine biomarker for kidney injury in experimental models and in clinical renal disease.

Keywords: biomarker; chronic kidney disease; epithelial–mesenchymal transition; periostin

Introduction

Chronic kidney disease (CKD) is emerging as a major global health threat [1]. Accurately assessing and monitoring renal function is critically important in CKD patients. The shortcomings of creatinine- and creatinine-derived equations have prompted the search for more reliable markers of kidney injury [2]. Ideally, novel CKD biomarkers should reflect mechanisms and activity of

continuing renal injury and predict disease progression and response to treatment.

Periostin, a member of the matricellular protein family, was initially identified in osteoblasts. Periostin acts as an adhesion molecule during bone formation, supports osteoblastic cell line attachment and is involved in cell survival, proliferation, migration and differentiation [3–6]. It is induced in diverse processes and pathologies including cardiac embryogenesis and adult disease, metastases, tumor suppression [7] and in proliferative diabetic retinopathy [8]. Evidence in these tissues suggests that periostin may play a fundamental role in tissue remodeling [9, 10] and in diseases of the cardiovascular system [11–13].

Periostin is induced during nephrogenesis, but it is not observed in normal adult kidney [14]. It also may accelerate cyst growth and promote interstitial remodeling in polycystic kidney disease (PKD) [15]. Information regarding periostin expression in kidney injury is still scant. This study reports on periostin expression and function in animal models of kidney disease and tubular cell culture and in CKD patients.

Materials and methods

Animals

Sprague–Dawley rats ($N = 18$) underwent 5/6 nephrectomy (Nx) ($n = 9$) by unilateral Nx and ligation of 2/3 of the vessels to the contralateral kidney or sham Nx. Rats were sacrificed 2 days, 2 weeks and 4 weeks after surgery. Microarray analysis was performed on the remnant nephron mass after 5/6Nx, including the infarct region. In order to examine exclusively non-infarcted tissue, additional experiments were performed for real-time-polymerase chain reaction (RT-PCR) studies only ($n = 3$ at each time point). The infarct was separated from non-infarcted tissue by visual inspection. A thin rim of normal tissue was excised with the infarct ensuring that only viable tissue was included in the specimen for study. In separate studies, diabetes was induced in DBA2J mice by intraperitoneal injection of streptozotocin 40 mg/kg/day for 5 days as described [16]. At 2 months, renal tissues were harvested. Finally, DBA2J mice underwent left unilateral ureteral obstruction (UUO) and kidneys were harvested at 5 and 14 days. All procedures were performed according to the guidelines established by the National Research Council Guide for the Care and Use of Laboratory Animals.

Gene array analysis

Affymetrix Gene Chip 230_2 expression analysis was used to compare the transcription profiles between normal kidneys and the remnant kidney (RK) 2 days and 2 and 4 weeks after 5/6Nx. Total RNA from three RK at each time point and three normal kidneys were labeled and hybridized to Affymetrix GeneChips. Data were expressed as average differences between the perfect match and mismatch probes for the periostin gene.

Human urine collection

Random urine samples were collected from healthy control volunteers ($n = 20$), proteinuric CKD patients ($n = 21$) and non-proteinuric CKD patients (PKD and hypertensive nephrosclerosis, $n = 24$) and stored at −80°C with protease inhibitors until assayed.

Quantitative RT-PCR analysis

Total RNA was isolated from rat control kidneys and RK at 2 days, 2 and 4 weeks after 5/6Nx and from DBA2J mouse control kidneys and streptozotocin-induced diabetic nephropathy (SZ-DN) at 2 months. RT-PCR with relative quantification of periostin copy number normalized to 18S ribosomal RNA transcripts was carried out using the following primers: periostin forward 5′-TGGTGTTGTCCATGTCATCGA-3′ and reverse 5′-TGTGAAGTGACCGTCTCTTCCA-3′. All polymerase chain reactions were run in an ABI 7900 Sequence Detection System (Applied Biosystems).

Immunohistochemistry

Four-micron sections of formalin-fixed paraffin-embedded tissue were deparaffinized and rehydrated. Endogenous peroxidase activity was quenched by incubation in endogenous enzyme block solution. Staining was performed at 4°C overnight with antibodies to polyclonal periostin (BioVendor, Candler, NC; 1:250), fibroblast-specific protein-1 (FSP1) (Abcam, Cambridge, MA; 1:100) and matrix metalloproteinase-9 (MMP9) (Chemicon, Temecula, CA; 1:100), followed by incubation with dextran polymer conjugated with horseradish peroxidase and affinity-isolated immunoglobulin for 30 min at room temperature. For controls, non-specific polyclonal IgG was used as primary antibody.

Immunofluorescence

Deparaffinized rat kidney sections prepared as described were double labeled with a primary rabbit polyclonal periostin antibody (BioVendor; 1:250) and either fluorescence-conjugated peanut agglutinin (PNA 5 μg/mL) lectin specific for distal nephron tubules (DT), fluorescence-conjugated phaseolus vulgaris erythroagglutinin (PHA-E) lectin (Vector Laboratories, Burlingame, CA; 1.5 μg/mL) specific for proximal nephron tubules and/or fluorescein isothiocyanate-conjugated monoclonal E-cadherin antibody (BD Biosciences, San Jose, CA; 1:200). In addition, using serial sections and PNA as a marker of DT, we compared the localization of periostin and E-cadherin in the DT. Indirect primary antibody was followed with goat anti-rabbit IgG conjugated to Texas Red (Santa Cruz Biotechnology, Santa Cruz, CA; 1:200). The PNA-positive tubules and the number that were both PNA and periostin positive were counted in eight randomly selected fields to calculate the percentage of DT that were periostin positive.

Immunoblotting analysis

Frozen kidney tissue and cell lysates were standardized by protein concentration, and a total of 30–100 μg of protein per well was loaded. Spot urine was collected from rats, patients and healthy volunteers. Two percent of the urinary volume for each rat sample and 0.03 mL for each human sample were subjected to immunoblotting as described previously [17].

Urine periostin analysis by enzyme-linked immunosorbent assay

Ninety-six-well microplates were coated overnight with 1 μg/mL (0.1 μg per well) of anti-periostin antibody (R&D Systems, Minneapolis, MN). Plates were washed three times with 0.05% Tween-20 in phosphate-buffered saline then blocked with reagent diluent for at least 1 h. One hundred microliter of all standards and patient samples was added to the 96-well plate and incubated for 2 h. After a 1-h incubation with rabbit polyclonal anti-periostin antibody (Abcam; 1:1000), 20-min incubation with dextran polymer conjugated with horseradish peroxidase and 20-min incubation with substrate solution, stop solution was added to each well. Periostin absorbance was calculated by measuring at 450 nm, correcting for plate artifact at 570 nm and utilizing a log-transformed standard curve.

Urine neutrophil gelatinase-associated lipocalin analysis by enzyme-linked immunosorbent assay

Urine neutrophil gelatinase-associated lipocalin (NGAL) enzyme-linked immunosorbent assay (ELISA) was performed using a commercially available assay (NGAL Rapid ELISA Kit 037; Bioporto, Grusbakken, Denmark) as per the manufacturer's protocol.

Generation of periostin-producing mouse distal collecting tubular cells and RNA interference

Full-length mouse periostin complementary DNA (cDNA) was subcloned into pCMV-SPORT6 (Thermo Scientific, Huntsville, AL). Plasmids were purified with the Qiagen Midiprep kit. One day before transfection, 6×10^5 immortalized mouse distal collecting tubular (MDCT) cells, kindly provided by Dr Peter Friedman, were plated in 60-mm culture dish wells overnight. Confluent cells (80–90%) were transfected with periostin construct or vector control. For periostin knockdown, cells were co-transfected with mouse periostin plasmid and SureSilencing short interfering RNA (siRNA) plasmid by using FuGENE HD transfection reagent, according to the manufacturer's instructions (Roche, Indianapolis, IN). After transfection for 24 h, cells were lysed and protein levels were determined by immunoblotting.

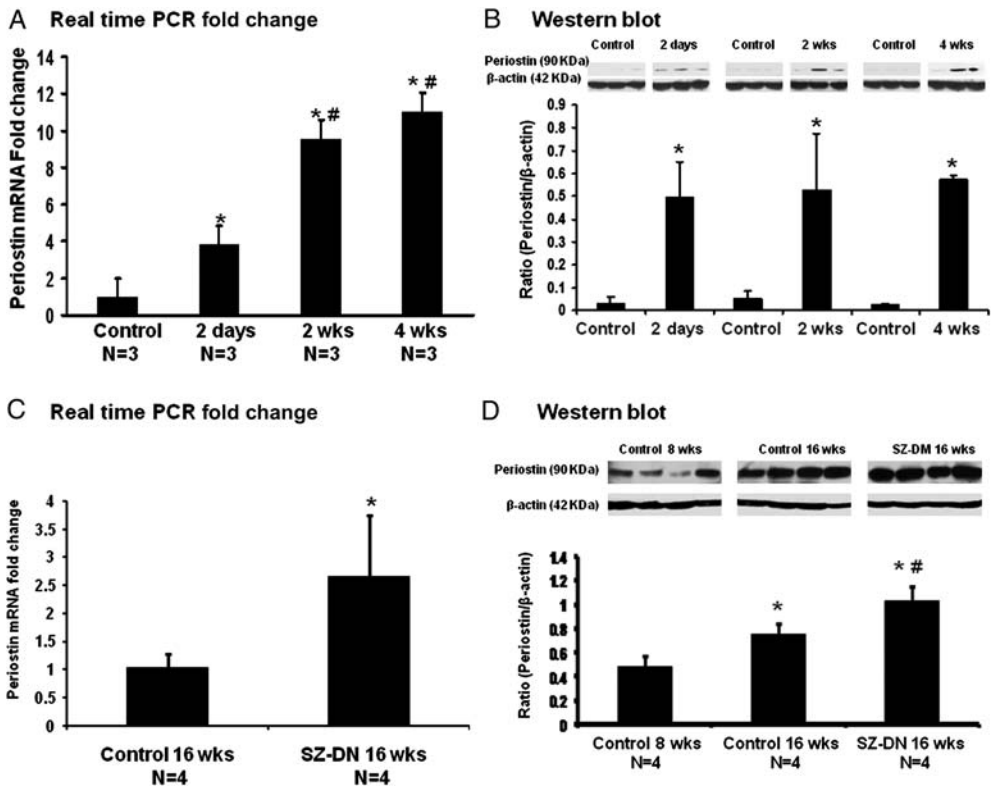

Fig. 1. Renal periostin increases after 5/6Nx in rats, SZ-DN and UUO in mice. (**A**) Periostin mRNA expression increased over time after 5/6Nx in RK compared to control kidney tissue in samples in which the infarct tissue was excised. The expression of 18S was used as an internal control. (**B**) Immunoblotting analysis for periostin was also increased in RK compared to control kidneys. *$P < 0.05$ versus control group, #$P < 0.05$ versus 2 days after 5/6Nx group. (**C**) Renal periostin mRNA expression increased after 2 months of streptozotocin injection in DBA2J mice compared to control kidneys. The expression of 18S was used as an internal control. *$P < 0.05$ versus control. (**D**) Renal periostin protein was increased in SZ-DN DBA2J mice compared to control DBA2J mice at 8 and 16 weeks. *$P < 0.05$ versus DBA2J mice control kidneys at 8 weeks, #$P < 0.05$ versus DBA2J mice control kidneys at 16 weeks.

Statistical analysis

Statistical analysis was performed using SPSS, version 15. Results are expressed as the mean ± SD. Two-sample *t*-test or Mann–Whitney rank-sum test was used for continuous variables. For multiple comparisons, analysis of variance was used followed by the least significant difference test. Spearman correlation coefficients were used as appropriate to test correlations between urine periostin and other variables. Receiver operating characteristics analysis was used to calculate the area under the curve (AUC) for urine periostin and NGAL and to find the best cutoff values for distinguishing healthy control values from CKD. $P < 0.05$ was considered statistically significant.

Results

Renal periostin messenger RNA and protein are increased after 5/6Nx in rats and with aging and SZ-DN in DBA2J mice

Microarray Gene Set Enrichment Analysis (GSEA; Broad Institute, Cambridge, MA) showed that periostin gene expression was significantly upregulated in the RK inclusive of the necrotic areas: 21.91-fold at Day 2, 13.32-fold at Week 2 and 14.46-fold at Week 4 when compared with control kidneys (data not shown). To confirm the microarray observation and to determine if periostin is expressed exclusively in the infarct, we examined periostin messenger RNA (mRNA) expression in separate RK tissues after infarct excision. RT-PCR showed a significant difference in periostin mRNA in the RK: 3.84-fold at Day 2 ($P = 0.025$), 9.57-fold at Week 2 ($P = 0.015$) and 11.05-fold at Week 4 ($P = 0.046$) versus control kidneys (Figure 1A). Immunoblotting corroborated the mRNA findings and showed increased periostin in RK compared to control kidneys (Figure 1B). Thus, the examination of periostin mRNA and protein in viable RK tissue without infarct unmasked a progressive increase in injured renal parenchyma after 5/6Nx. In order to ascertain whether periostin is increased in renal injury lacking ischemia and infarction, periostin mRNA and protein were measured in diabetic DBA2J mice. RT-PCR performed on renal tissue 2 months after streptozotocin or diluent injections showed a 2.66-fold increase in renal periostin mRNA in SZ-DN compared to controls ($P = 0.011$) (Figure 1C). DBA2J mice develop albuminuria with aging. Immunoblotting demonstrated a significant increase in renal periostin both in aging DBA2J mice (8 versus 16 weeks) and between age-identical DBA2J mice with and without SZ-DN (Figure 1D). Taken together, the data show that periostin mRNA and protein are increased after 5/6Nx, in aging DBA2J mice and in SZ-DN.

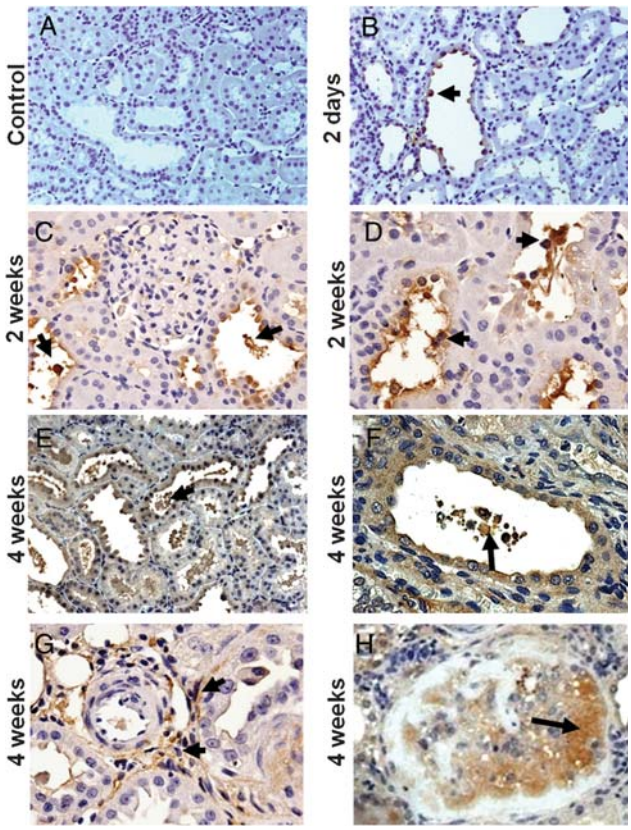

Fig. 2. Renal periostin immunostaining after 5/6Nx in rats. (**A**) Periostin immunostaining was not detected in cortical control rat kidney. (**B**–**H**) In contrast, representative sections of kidney tissues at 2 days, 2 and 4 weeks displayed cytoplasmic staining for periostin, most prominently in the apical portion of tubular cells (B arrow), with stronger and more diffuse tubular cell staining at 2 and 4 weeks. There also was periostin staining in casts and/or in sloughed cells in the tubular lumina (C, D, E, F arrows) (A–F original magnification: ×400). (G) Four weeks after 5/6Nx, periostin was present in the interstitium (arrows), frequently in the periadventitial area around arteries and arterioles. (Original magnification: ×400). (H) There was periostin staining in an extracellular distribution in glomeruli undergoing obsolescence (original magnification: ×100).

Renal periostin immunohistochemistry demonstrates increments after 5/6Nx in rats, in DBA2J mice with aging and SZ-DN and after UUO

Periostin immunostaining was not detected in cortical control rat kidney (Figure 2A). In contrast, representative sections of kidney 2 days and 2 and 4 weeks after 5/6Nx show cytoplasmic periostin staining, most prominently in the apical portion of tubular cells, faintly at 2 days and more strongly with more diffuse tubular cell staining at 2 and 4 weeks. Detached tubular cells and cytoplasmic cell fragments sloughed into tubular lumina frequently were positive for periostin (Figure 2C–F). At 4 weeks, periostin-positive interstitial cells were frequent in periadventitial areas around arteries and arterioles (Figure 2G). Periostin was also present in the extracellular matrix of glomeruli undergoing obsolescence (Figure 2H). These data demonstrated concordance between mRNA and protein changes observed after 5/6Nx in tubules in the non-infarcted regions of the RK.

A similar distribution and increment in periostin were also detected by immunohistochemistry in aging compared to younger DBA2J mice (Figure 3A and B). Even more periostin staining was noted when SZ-DN was superimposed on aging in DBA2J mice (Figure 3B and C). In both aging and SZ-DN, prominent periostin staining was identified. In aging, it was patchy, but in aging plus SZ-DN, staining was noted diffusely in tubular cell cytoplasm.

Finally, in DBA2J mice after UUO, similar tubular cytoplasmic staining for periostin was demonstrated, increasing in intensity and distribution with time after ureteral ligation (Figure 3D–F). Taken together, these data demonstrated that renal tubular periostin expression appeared to be a general response to varied renal injuries.

Periostin is expressed in DT

Periostin was expressed in the cytoplasm of tubular epithelial cells that also stained positively for PNA lectin, indicating expression in DT. There was an average of 20 positive tubules per h.p.f. (range 15–31) and 10 double-staining PNA and periostin-positive tubules per h.p.f. (range 6–15). Approximately 49% of the PNA-positive tubules (range 38–60%) were also periostin positive. No periostin was identified in nephron segments stained with the proximal tubular lectin marker PHA-E. Thus, periostin localized to the DT in the RK (Figure 4).

Disappearance of the tight junction protein E-cadherin in DT expressing periostin

Using serial sections, immunofluorescence analysis of the RK demonstrated that DT retained their affinity for PNA lectin whether the tubules did or did not express periostin. However, in PNA lectin-positive DT, the expression of E-cadherin and periostin was virtually mutually exclusive (Figure 5A–D). These studies demonstrated an association between the appearance of periostin in DT in the RK concomitant with the disappearance of the DT protein E-cadherin, the latter a marker of the tubular differentiated state and a transmembrane protein responsible for cell–cell adhesion.

Periostin expression in tubular epithelium associates with the appearance of epithelial–mesenchymal transition markers

To study tubular dedifferentiation, serial sections of renal tissue after 5/6Nx were stained for periostin (Figure 6A, D, G and J); FSP1 (Figure 6B, E, H and K), a cytoplasmic marker of epithelium undergoing mesenchymal transition and MMP9 (Figure 6C, F, I and L), a protein involved in the turnover of extracellular matrix in tissue remodeling. These immunohistochemical studies revealed co-staining of MMP9 and FSP1 with periostin in affected DT cells, including sloughed cells and cytoplasmic fragments in tubular lumina, at all time points after 5/6Nx. Interstitial cells stained occasionally for periostin, FSP1 and MMP9 at 2 weeks (Figure 6D–F), with more extensive interstitial staining at 4 weeks (Figure 6G–L). These studies demonstrate an association between periostin expression and changes in specific proteins in renal

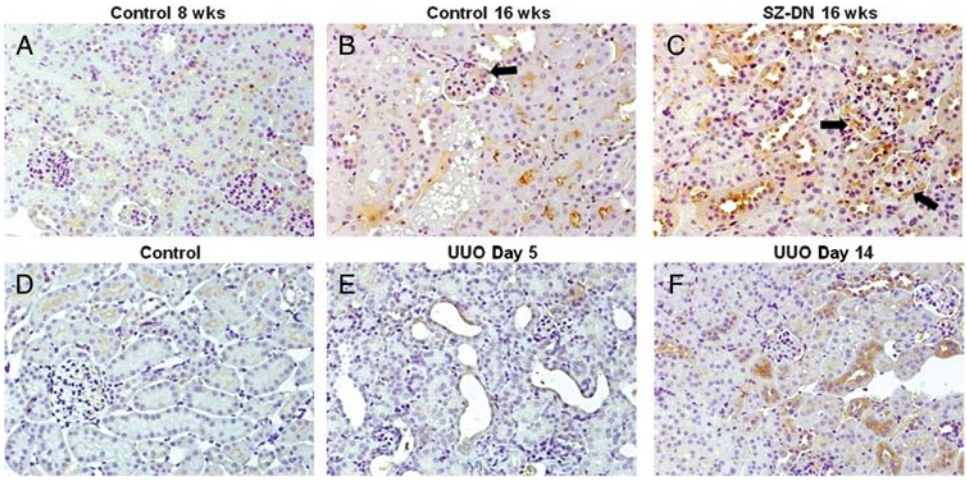

Fig. 3. Renal periostin immunostaining after diabetes induction, in aging, and after UUO in mice. (**A**) Control DBA2J mouse kidneys with faint periostin staining at 8 weeks. (**B**) There is focal apical tubular and infrequent glomerular (arrow) periostin staining in aging 16-week-old DBA2J mice. (**C**) There is a marked increase in tubular and focal increase in glomerular (arrows) periostin immunostaining of 16-week-old DBA2J mice with SZ-DN for 2 months. (**D**) Control sham-operated DBA2J mouse kidney with minimal periostin staining. (**E**) Tubular injury and mild focal increase in tubular epithelial cell periostin immunostaining after UUO at 5 days. (**F**) At 14 days after UUO, there is a marked increase in tubular cell periostin. (Original magnification: ×200).

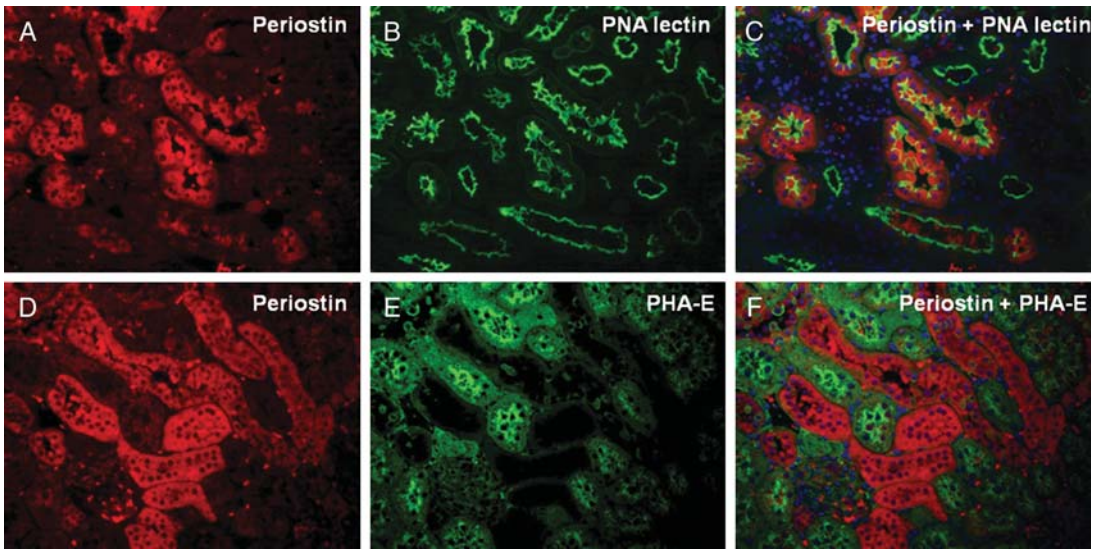

Fig. 4. Periostin localizes exclusively to tubular cells of the distal nephron after 5/6Nx. Paraffin-embedded sections were double labeled with anti-periostin antibody (red; **A**, **D**) and either distal nephron marker PNA lectin (green; **B**) or proximal nephron marker PHA-E lectin (green; **E**). Periostin co-localized with PNA staining exclusively in the distal nephron (**C**), but never with PHA-E staining in the proximal nephron (**F**). Merged images show periostin in red and PNA or PHA-E in green (original magnification: ×200). Cell nuclei were stained with 4′,6-diamidino-2-phenylindole (C and F).

tubules indicating loss of at least one differentiation marker of tubular epithelium (E-cadherin) and expression of two markers characteristic of a mesenchymal phenotype (FSP1 and MMP9).

In vitro, periostin overexpression induces and periostin siRNA represses, a mesenchymal phenotype in MDCT cells

We used a transfection system to introduce periostin cDNA into MDCT cells. MDCT cells overexpressing periostin dramatically increased MMP9 and FSP1 expression, hallmarks for mesenchymal cells. The levels of MMP9 and FSP1 in parental MDCT cells and vector-transfected control cells were barely detectable. In contrast, expression of the tight- junction protein E-cadherin was strikingly diminished in periostin-producing cells, and FSP1 and MMP9 proteins were increased (Figure 7A). Gene knockdown with siRNA was next applied to further analyze the effect of periostin. MDCT cells co-transfected with periostin cDNA and siRNA showed obviously reduced periostin protein

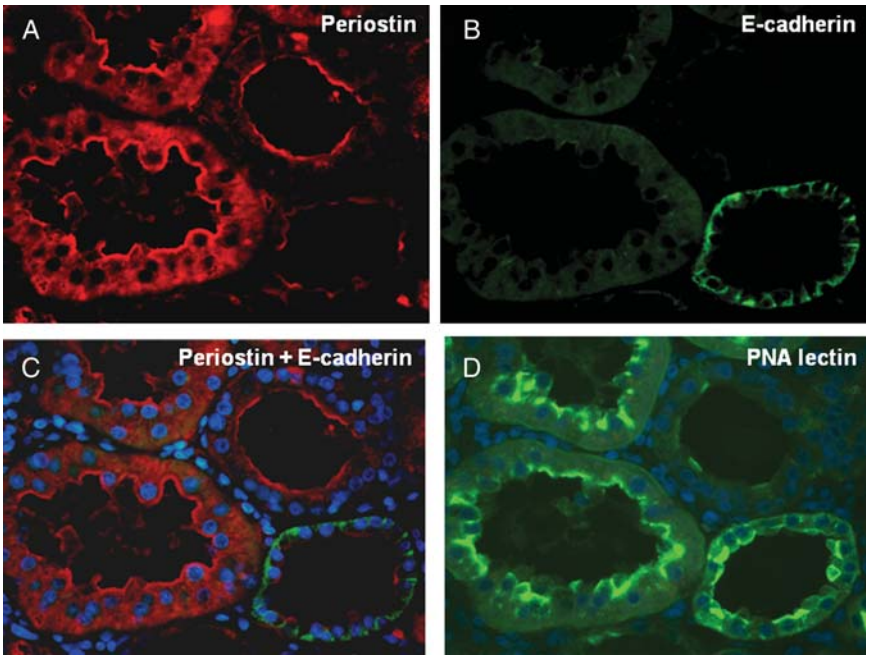

Fig. 5. Disappearance of the tight junction protein E-cadherin in DT expressing periostin. E-cadherin expression is lost in distal nephron tubules expressing cytoplasmic periostin after 5/6Nx. Serial sections show virtually mutually exclusive immunofluorescence staining patterns for cytoplasmic periostin (red; **A**) and E-cadherin (green; **B**) in RK tissues 4 weeks after 5/6Nx. The section was counterstained with 4′,6-diamidino-2-phenylindole to visualize tubule cell nuclei (merge; **C**). Sequential sections also show that tubules expressing either periostin or E-cadherin both continued to express PNA lectin (**D**), demonstrating that both are being expressed in distal nephron tubules.

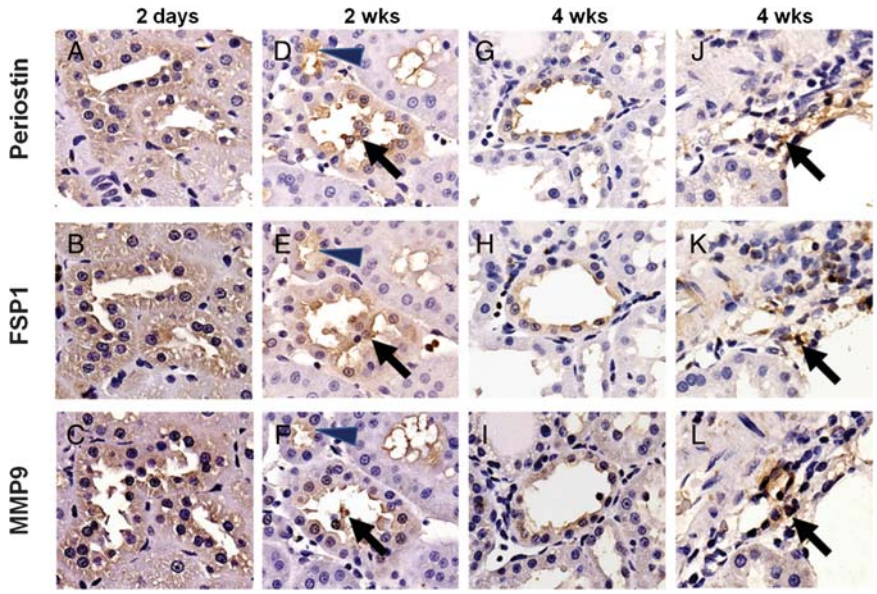

Fig. 6. Periostin induces a mesenchymal phenotype. Periostin, FSP1 and MMP9 are co-expressed in RK 2 days, 2 and 4 weeks after 5/6Nx. Serial sections of RK were stained for periostin (**A**, **D**, **G**, **J**), FSP1 (**B**, **E**, **H**, **K**) and MMP9 (**C**, **F**, **I**, **L**) at 2 days (A–C); 2 weeks (D–F) and 4 weeks (G–L) after 5/6Nx. (A–I) Staining of MMP9 and FSP1 shows co-localization with periostin in renal tubular epithelium, in luminal sloughed tubular cells and in luminal cytoplasmic fragments at all times after 5/6Nx. (D, E, F) Sequential serial sections demonstrate sloughed luminal cells cut at different levels causing variation in shape and volume; however, all sections contain cell cytoplasm staining for periostin, FSP1 and MMP9 (arrows). Intact tubular cells, which are larger and therefore more easily identified as the same cell across all sections, also demonstrate co-expression of all proteins (arrowheads). (Original magnification: ×600). (J–L) Interstitial cells in the 4-week RK also stain for periostin, FSP1 and MMP9 (arrows) (original magnification: ×400).

levels. The effect of periostin on renal tubular MMP9 and FSP1 generation and E-cadherin reduction was blocked by periostin siRNA transfection (Figure 7B). In the aggregate, the data demonstrate that periostin expression in MDCT cells induces the expression of mesenchymal characteristics.

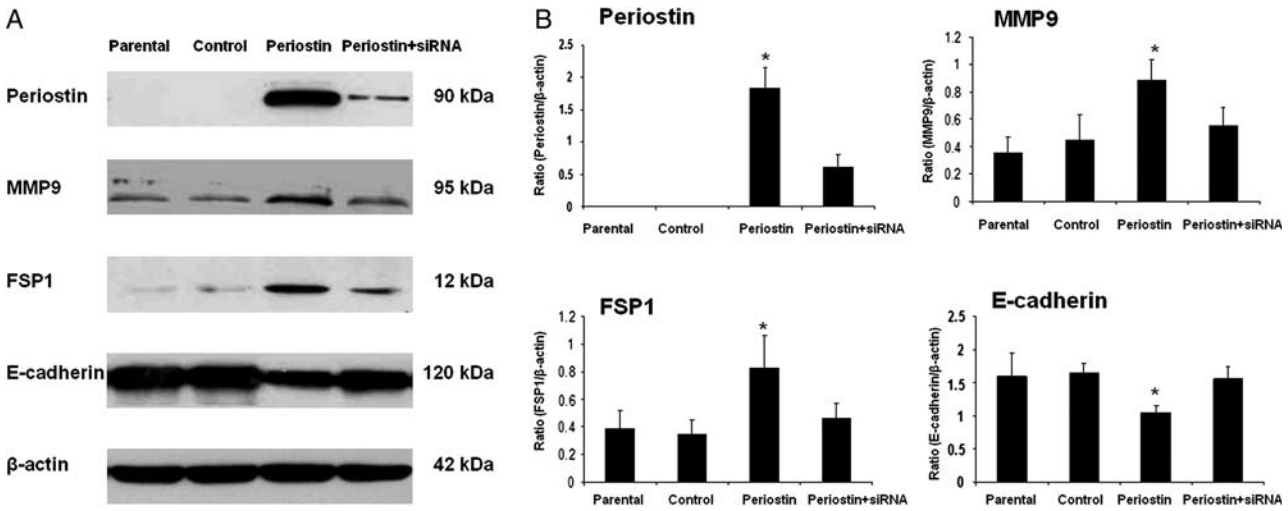

Fig. 7. Cells overexpressing periostin express mesenchymal markers. Cell lysates from parental cells, cells trasfected with empty vector (control), transfected periostin vector cells, and cells co-transfected with periostin and SureSilencing periostin siRNA were employed to examine periostin, MMP9, FSP1 and E-cadherin expression. (**A**) Representative western immunoblots showing that MDCT cells expressing periostin dramatically increased MMP9 and FSP1 expression, hallmarks of a mesenchymal phenotype. E-cadherin expression was reduced in the periostin overexpressing cells. Co-transfected periostin and SureSilencing siRNA vector cells expressed reduced levels of periostin protein. Reduced periostin expression resulted in restoration of E-cadherin and partial reduction of MMP9 and FSP1 expression. (**B**) Quantification of western immunoblotting results. *P < 0.05 versus parental, control and periostin + siRNA group.

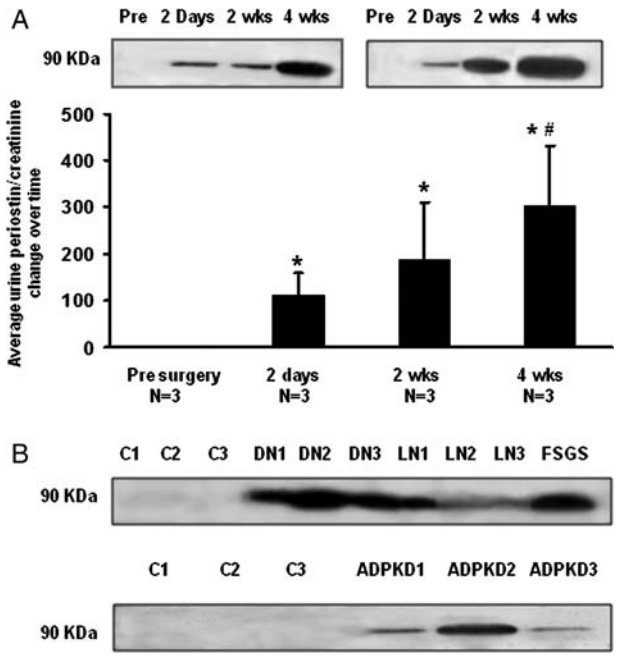

Fig. 8. Urine periostin excretion rate increment after 5/6Nx in the RK model of progressive renal injury and in patients with proteinuric and non-proteinuric renal diseases. (**A**) Western blotting analysis for urine periostin was performed on individual rats prior to 5/6Nx and after 2 days, 2 and 4 weeks ($n = 3$ at each time point). Each lane was loaded with 2% of the total urinary flow rate for each rat. Urine creatinine was measured and used to control for concentration. Representative western blots are shown. Experiments were performed in triplicate. *P < 0.05 versus pre-surgery group, #P < 0.05 versus 2 days after 5/6Nx group. (**B**) In lightly centrifuged urine treated and stored with protease inhibitors, then thawed for the assay, 90-kDa urine periostin was detectable in patients with various proteinuric glomerular diseases, but not in controls (0.03 mL urine). With urine collected identically, in patients with non-proteinuric PKD but not in controls, 90-kDa urine periostin is also clearly detectable. C, control; DN, diabetic nephropathy; LN, lupus nephritis; FSGS, focal and segmental glomerulosclerosis.

Urinary periostin excretion progressively increased over time after 5/6Nx

Figure 8A shows the time course for the excretion of urine periostin before and after 5/6Nx in a longitudinal experiment in which urine was collected from the same animals serially until their sacrifice at 4 weeks. Urine periostin was undetectable before 5/6Nx. There were significant incremental increases in urine periostin excretion over time after 5/6Nx. These data show that urine periostin distinguished healthy from injured kidney categorically and excretion increased over time with chronicity of injury.

Human urine periostin is detectable by immunoblotting in CKD patients

Urine periostin is detectable both in proteinuric and non-proteinuric CKD patients (Figure 8B) but not in healthy controls, underscoring its value as a potential biomarker for kidney injury in proteinuric and non-proteinuric conditions.

Using a quantitative ELISA, urine periostin is higher in proteinuric and non-proteinuric CKD patients than in healthy controls

A standard curve was generated using known concentrations of recombinant periostin resulting in a linearized R^2 of 0.981 (data not shown). Table 1 describes the clinical characteristics of the patients. Urine periostin was measured by ELISA in proteinuric CKD ($n = 21$) and non-proteinuric CKD ($n = 24$) and in healthy controls ($n = 20$). Two additional patients had non-progressive CKD [minimal-change nephropathy (MCD) and Wegener's granulomatosis in remission]. The mean estimated glomerular filtration rate for CKD subjects is shown, subdivided by diagnostic category. The number of subjects

Table 1. Clinical characteristics of the patients with proteinuric and non-proteinuric CKD[a]

Etiology of CKD	Mean age (years)	Gender	Serum albumin (g/dL)	BUN (mg/dL)	Serum creatinine (mg/dL)	UPCR	eGFR (mL/min/1.73m^2)
Proteinuric patients (n = 21)	46.1 ± 14.2	F = 7, M = 14	3.1 ± 0.8	49.3 ± 26.3	3.1 ± 1.7	4.6 ± 2.8	35.4 ± 34.1
DN (n = 13)	52.5 ± 10.3	F =2, M = 11	3.4 ± 0.5	60.8 ± 19.9	3.7 ± 1.5	4.0 ± 1.9	20.4 ± 6.9
GN (n = 8)	35.8 ± 14.7	F = 5, M = 3	2.6 ± 1.1	30.5 ± 25.4	2.2 ± 1.7	5.7 ± 3.8	59.9 ± 46.1
LN (n = 2)	20.5 ± 2.1	F, M	2.5 ± 0.0	46.0 ± 46.7	2.9 ± 3.1	4.2 ± 1.4	9.9 ± 62.9
MN (n = 3)	1.0 ± 14.4	F = 2, M	2.5 ± 1.2	31.6 ± 18.0	2.7 ± 1.4	7.0 ± 1.6	34.8 ± 31.2
IgMN (n = 2)	35.5 ± 17.7	F = 2	2.6 ± 2.1	7.5 ± 4.9	0.7 ± 0.2	7.4 ± 7.8	113.4 ± 20.8
FSGS (n = 1)	51.0	M	3.3	42.0	2.5	1.6	28.6
Non-proteinuric patients (n = 24)	62.1 ± 4.4	F=7, M = 17	4.2 ± 0.4	25.8 ± 13.5	2.0 ± 1.3	0.1 ± 0.1	40.1 ± 19.1
HTN (n = 19)	67.4 ± 9.5	F = 4, M = 15	4.4 ± 0.3	22.4 ± 7.5	1.7 ± 0.4	0.1 ± 0.1	43.1 ± 16.7
PKD (n = 5)	42.2 ± 12.8	F = 3, M = 2	3.6 ± 0.3	39.0 ± 22.7	3.6 ± 2.4	0.4 ± 0.2	28.7 ± 24.8

BUN, blood urea nitrogen; UPCR, urine protein creatinine ratio; eGFR, estimated glomerular filtration rate; DN, diabetic nephropathy; HTN, hypertensive nephropathy; LN, lupus nephritis; MN, membranous nephropathy; IgMN, IgM nephropathy; FSGS, focal and segmental glomerulosclerosis.

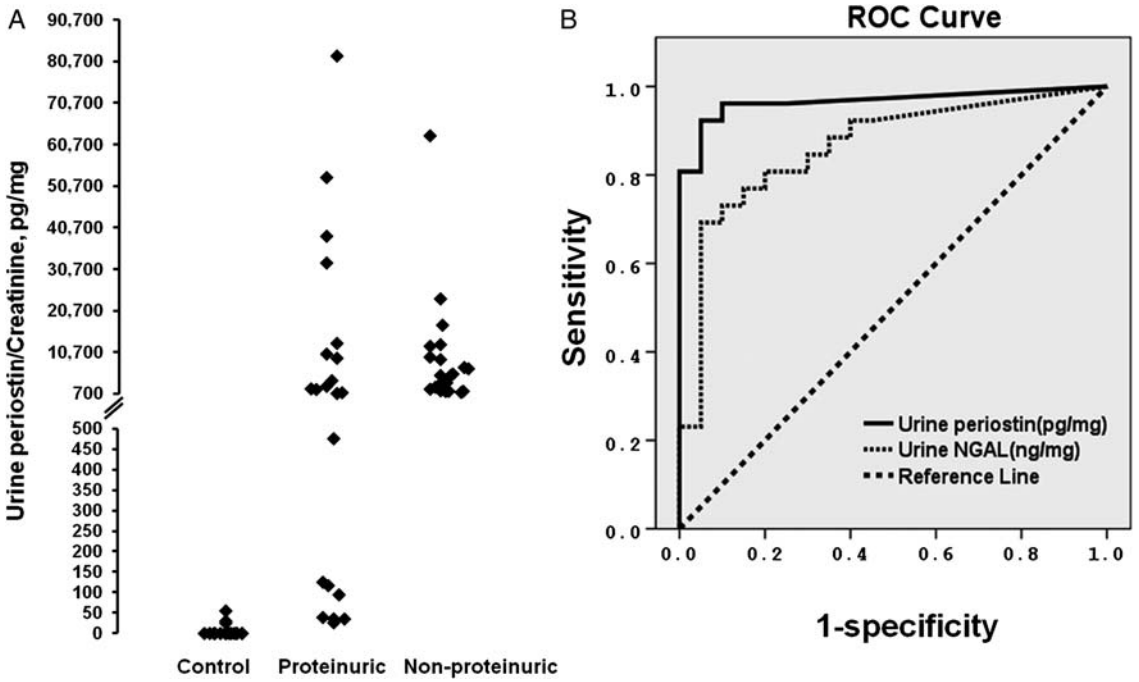

Fig. 9. Urine periostin ELISA distinguishes CKD from healthy controls with high sensitivity and specificity. (**A**) Urine periostin/creatinine measured by ELISA is higher in patients with progressive proteinuric renal disease (n = 21) and non-proteinuric renal disease (n = 24) than in healthy controls (n = 20). Individual values for each patient and control represents the average of at least triplicate testing. The median values for patients with progressive proteinuric disease (2473.58 pg/mg) and non-proteinuric renal disease (3192.36 pg/mg) were not significantly different, but each was significantly higher than for healthy controls (0 pg/mg). (**B**) Receiver operating characteristics curves of urinary periostin and NGAL considering CKD as the status variable (controls, proteinuric CKD and PKD). The AUC for urinary periostin and NGAL was 0.96 (95% CI, 0.91–1.02) and 0.86 (95% CI, 0.75–0.97), respectively. Both urinary periostin and NGAL areas were statistically different with respect to that of the diagnostic reference line (P < 0.001). The difference between the two biomarker areas was not significant (P = 0.09).

according to CKD stage was CKD 1 (n = 3); CKD 2 (n = 6); CKD 3 (n = 11); CKD 4 (n = 18) and CKD 5 (n = 7). The median urine periostin in healthy controls (0 pg/mg) was significantly less than in patients with proteinuric CKD (2473.58 pg/mg, P < 0.001) and non-proteinuric CKD (3192.36 pg/mg, P < 0001) (Figure 9A). There was no significant difference between the median values in the patients with proteinuric and non-proteinuric CKD (P = 0.21), supporting the proposition that periostin is not filtered and its urinary source is tubular. These data support the proposition that urine periostin is an indicator of active tubular injury and is not a reflection of glomerular injury nor the direct result of albuminuria.

Urinary periostin demonstrates high specificity and sensitivity for diagnosing CKD

Urine periostin and NGAL were measured by ELISA and corrected for urine creatinine. AUC for urine periostin/cr and urine NGAL/cr were 0.96 [95% confidence interval

(CI), 0.91–1.02] and 0.86 (95% CI, 0.75–0.97), respectively (Figure 9B). Urine periostin/cr and NGAL/cr AUC were both statistically different from the reference line ($P < 0.001$), but similar to each other ($P = 0.09$). For urine periostin/cr, the best cutoff level was 32.66 pg/mg (sensitivity 92.3% and specificity 95.0%), whereas for urine NGAL/cr, it was 13.73 ng/mg (sensitivity 80.8% and specificity 80.0%). Thus, the urine periostin/cr measurement demonstrated high sensitivity and specificity for diagnosing CKD and compared favorably with urine NGAL/cr.

Discussion

This study describes the renal expression and urine excretion of periostin in experimental models of renal disease and in the urine of CKD patients. Urine periostin/cr demonstrated high sensitivity and specificity for diagnosing CKD comparing favorably with urine NGAL/cr. *In vivo* and *in vitro*, DT cells expressing periostin also expressed other mesenchymal proteins such as FSP1 and MMP9 *de novo*, but lost E-cadherin. Moreover, in MDCT cells transfected to overexpress periostin, concomitant periostin siRNA transfection attenuated these changes. Taken together, these data demonstrate that periostin promotes the expression of a mesenchymal phenotype in renal tubule cells and is a promising tissue and urine biomarker for distal tubular cell injury.

Periostin, originally identified in osteoblasts, is a cell adhesion molecule for pre-osteoblasts and participates in osteoblast recruitment and spreading [3–6]. Periostin may contribute to renal tissue remodeling in a manner analogous to its functions in other injured tissues [18, 19]. In our study, periostin staining in RK was abundant in DT, increased in intensity and distribution with time after renal injury and was noted predominantly in the renal tubular epithelial cell cytoplasm and in tubular epithelial cells shed into the lumen. Less commonly, periostin was identified in the extracellular matrix of glomeruli undergoing obsolescence and in periadventitial areas surrounding arteries and arterioles. This intracellular localization distinguishes our findings somewhat from other published observations in kidney and other tissues. Consistent with our findings, periostin is not reported in normal kidney [15]. However, in PKD, periostin was localized sparsely within cyst epithelial cells, was found predominantly in the interstitium lining the basal surface of most cysts [15] and was secreted into PKD cyst fluid. Nevertheless, our finding of intracellular periostin is not unique. Cytoplasmic periostin has been reported in M3T3-E1 osteoblast-like cells in culture [20]. In COS-7 cells overexpressing periostin [21], and endogenously in a human corneal fibroblast cell line, periostin localized intracellulary in the secretory apparatus of the trans-Golgi network [21]. It has also been identified in an intracellular pattern in human lung cancer cells [22], human breast cancer [23] and in normal corneal epithelium [21]. One may speculate that cytoplasmic periostin accumulation in injured distal tubule cells represents a failure of the cell secretory system, a hypothesis requiring confirmation by experimentation. Thus, the data suggest that the *de novo* expression of periostin during injury and its excretion in urine are common events during progressive renal functional decline.

The term epithelial–mesenchymal transition (EMT) has been used to describe the hypothesis that transformed tubular epithelial cells are the source of interstitial fibroblasts [24], a hypothesis that has recently been refuted [25]. Nevertheless, the studies reported herein show that periostin upregulation due to injury *in vivo* and due to transfection *in vitro* is associated with and/or directly induce tubule cells to express mesenchymal proteins and to lose the expression of a differentiated epithelial cell protein. It is appropriate to describe this adoption of mesenchymal characteristics as EMT. Many reports describe periostin overexpression in malignant cells that had undergone EMT and metastasized [26–28]. In addition, one study showed that periostin overexpression in a tumorigenic epithelial cell line-induced fibroblast-like transformation with increased expression of vimentin, epidermal growth factor receptor, MMP9 and evidence for increased cell migration and adhesion, indicative of EMT [29]. In agreement with these previously reported studies conducted on neoplastic tissues, this study also demonstrates that periostin overexpression in cultured MDCT cells dramatically induced the appearance of the mesenchymal markers MMP9 and FSP1 and a decrement in the epithelial cell marker E-cadherin. The combination of increased MMP9 degrading basement membrane and decreased E-cadherin diminishing cell–cell adhesion likely contributes to DT cell sloughing and indicates that renal tubular cell periostin expression is a marker of EMT. Our study confirms that tubular cells undergoing injury do acquire a mesenchymal phenotype, but in this process, they appear to be at risk of losing cell–cell and cell–matrix attachments and slough into the tubular lumen, more so than migrating into the interstitium.

Our experiments do not address how periostin enters the urine. In teeth, heart and in PKD, periostin is a secreted protein and is part of the extracellular matrix [15, 30, 31]. Our work shows periostin expressed predominantly in tubule epithelial cell cytoplasm, suggesting that cell injury impairs its secretion. Thus, one may speculate that periostin may enter the urine either by residual secretory capacity of tubule epithelial cells or by direct release from degenerating sloughed cells. In the aggregate, our data suggest that the periostin measured in the urine is derived mostly or entirely from a renal tubular source. However, the data do not definitively exclude the possibility that some fraction of the excreted periostin may be derived from glomerular filtration. Only measurements of the filtration of labeled periostin can address this question directly, and these studies have not yet been performed.

In conclusion, these studies demonstrate that urine periostin is a CKD biomarker that reflects the adoption of a mesenchymal phenotype by distal renal tubular cells in response to diverse renal injuries across species. Its renal histopathological expression patterns and its coordinated effect on the induction of a mesenchymal phenotype when overexpressed *in vitro* suggest that periostin may be a biomarker that also participates in the pathogenesis of CKD.

Acknowledgements. We are grateful for grant support from the National Kidney Foundation of Southern California, the International Society of Nephrology, the National Kidney Foundation of Thailand and the Los Angeles Biomedical Research Institute GCRC (M01–RR00425).

Conflict of interest statement. None declared.

References

1. Levey AS, Atkins R, Coresh J *et al*. Chronic kidney disease as a global public health problem: approaches and initiatives—a position statement from Kidney Disease Improving Global Outcomes. *Kidney Int* 2007; 72: 247–259.
2. Vassalotti JA, Stevens LA, Levey AS. Testing for chronic kidney disease: a position statement from the National Kidney Foundation. *Am J Kidney Dis* 2007; 50: 169–180.
3. Horiuchi K, Amizuka N, Takeshita S *et al*. Identification and characterization of a novel protein, periostin, with restricted expression to periosteum and periodontal ligament and increased expression by transforming growth factor beta. *J Bone Miner Res* 1999; 14: 1239–1249.
4. Takeshita S, Kikuno R, Tezuka K *et al*. Osteoblast-specific factor 2: cloning of a putative bone adhesion protein with homology with the insect protein fasciclin I. *Biochem J* 1993; 294 (Pt 1): 271–278.
5. Lindner V, Wang Q, Conley BA *et al*. Vascular injury induces expression of periostin: implications for vascular cell differentiation and migration. *Arterioscler Thromb Vasc Biol* 2005; 25: 77–83.
6. Li G, Oparil S, Sanders JM *et al*. Phosphatidylinositol-3-kinase signaling mediates vascular smooth muscle cell expression of periostin in vivo and in vitro. *Atherosclerosis* 2006; 188: 292–300.

7. Coutu DL, Wu JH, Monette A *et al*. Periostin, a member of a novel family of vitamin K-dependent proteins, is expressed by mesenchymal stromal cells. *J Biol Chem* 2008; 283: 17991–18001.
8. Takada M, Ban Y, Yamamoto G *et al*. Periostin, discovered by nanoflow liquid chromatography and mass spectrometry, is a novel marker of diabetic retinopathy. *Biochem Biophys Res Commun* 2010; 399: 221–226.
9. Kruzynska-Frejtag A, Wang J, Maeda M *et al*. Periostin is expressed within the developing teeth at the sites of epithelial-mesenchymal interaction. *Dev Dyn* 2004; 229: 857–868.
10. Rani S, Barbe MF, Barr AE *et al*. Periostin-like-factor and periostin in an animal model of work-related musculoskeletal disorder. *Bone* 2009; 44: 502–512.
11. Litvin J, Blagg A, Mu A *et al*. Periostin and periostin-like factor in the human heart: possible therapeutic targets. *Cardiovasc Pathol* 2006; 15: 24–32.
12. Katsuragi N, Morishita R, Nakamura N *et al*. Periostin as a novel factor responsible for ventricular dilation. *Circulation* 2004; 110: 1806–1813.
13. Norris RA, Kern CB, Wessels A *et al*. Identification and detection of the periostin gene in cardiac development. *Anat Rec A Discov Mol Cell Evol Biol* 2004; 281: 1227–1233.
14. Ito T, Suzuki A, Imai E *et al*. Tornado extraction: a method to enrich and purify RNA from the nephrogenic zone of the neonatal rat kidney. *Kidney Int* 2002; 62: 763–769.
15. Wallace DP, Quante MT, Reif GA *et al*. Periostin induces proliferation of human autosomal dominant polycystic kidney cells through alphaV-integrin receptor. *Am J Physiol Renal Physiol* 2008; 295: F1463–F1471.
16. Dai T, Patel-Chamberlin M, Natarajan R *et al*. Heat shock protein 27 overexpression mitigates cytokine-induced islet apoptosis and streptozotocin-induced diabetes. *Endocrinology* 2009; 150: 3031–3039.
17. Dai T, Natarajan R, Nast CC *et al*. Glucose and diabetes: effects on podocyte and glomerular p.38MAPK, heat shock protein 25, and actin cytoskeleton. *Kidney Int* 2006; 69: 806–814.
18. Oku E, Kanaji T, Takata Y *et al*. Periostin and bone marrow fibrosis. *Int J Hematol* 2008; 88: 57–63.
19. Takayama G, Arima K, Kanaji T *et al*. Periostin: a novel component of subepithelial fibrosis of bronchial asthma downstream of IL-4 and IL-13 signals. *J Allergy Clin Immunol* 2006; 118: 98–104.
20. Litvin J, Selim AH, Montgomery MO *et al*. Expression and function of periostin-isoforms in bone. *J Cell Biochem* 2004; 92: 1044–1061.
21. Kim BY, Olzmann JA, Choi SI *et al*. Corneal dystrophy-associated R124H mutation disrupts TGFBI interaction with Periostin and causes mislocalization to the lysosome. *J Biol Chem* 2009; 284: 19580–19591.
22. Soltermann A, Tischler V, Arbogast S *et al*. Prognostic significance of epithelial-mesenchymal and mesenchymal-epithelial transition protein expression in non-small cell lung cancer. *Clin Cancer Res* 2008; 14: 7430–7437.
23. Puglisi F, Puppin C, Pegolo E *et al*. Expression of periostin in human breast cancer. *J Clin Pathol* 2008; 61: 494–498.
24. Iwano M, Plieth D, Danoff TM *et al*. Evidence that fibroblasts derive from epithelium during tissue fibrosis. *J Clin Invest* 2002; 110: 341–350.
25. Humphreys BD, Lin SL, Kobayashi A *et al*. Fate tracing reveals the pericyte and not epithelial origin of myofibroblasts in kidney fibrosis. *Am J Pathol* 2010; 176: 85–97.
26. Gillan L, Matei D, Fishman DA *et al*. Periostin secreted by epithelial ovarian carcinoma is a ligand for alpha(V)beta(3) and alpha(V)beta (5) integrins and promotes cell motility. *Cancer Res* 2002; 62: 5358–5364.
27. Sasaki H, Sato Y, Kondo S *et al*. Expression of the periostin mRNA level in neuroblastoma. *J Pediatr Surg* 2002; 37: 1293–1297.
28. Ruan K, Bao S, Ouyang G. The multifaceted role of periostin in tumorigenesis. *Cell Mol Life Sci* 2009; 66: 2219–2230.
29. Yan W, Shao R. Transduction of a mesenchyme-specific gene periostin into 293T cells induces cell invasive activity through epithelial-mesenchymal transformation. *J Biol Chem* 2006; 281: 19700–19708.
30. Kii I, Amizuka N, Minqi L *et al*. Periostin is an extracellular matrix protein required for eruption of incisors in mice. *Biochem Biophys Res Commun* 2006; 342: 766–772.
31. Snider P, Hinton RB, Moreno-Rodriguez RA *et al*. Periostin is required for maturation and extracellular matrix stabilization of noncardiomyocyte lineages of the heart. *Circ Res* 2008; 102: 752–760.

Received for publication: 12.9.2010; Accepted in revised form: 20.10.2011